Ultrasound Segmentation in Navigated Liver Surgery

Sylvain Anderegg, Matthias Peterhans, Stefan Weber

University of Bern, Institute for Surgical Technology & Biomechanics (ISTB), Bern, Switzerland

Contact: matthias.peterhans@istb.unibe.ch

Abstract:

In computer assisted liver surgery, the use of pre-operative 3D computer tomography (CT) images provides basic orientation and valuable information about the patient liver. During the surgical intervention, the accuracy of this information is reduced by motion and deformation of the organ. The fusion of intra-operative ultrasound (US) imaging with the pre-operative data is the next step in order to improve this situation. As pre-requisite, the identification of corresponding structures in US and CT (such as blood vessels) is required. Within this paper, the integration of an ultrasound vessel segmentation algorithm in a navigation system for liver surgery is presented. Initial results obtained on patients undergoing liver resection are evaluated.

Keywords: Liver surgery, Ultrasound segmentation, Computer assisted surgery

1 Problem

Intra-operative ultrasound imaging is used during surgical interventions on the open liver, providing real-time information about the organ inner structure. Moreover, new tumors may be detected and the surgical intervention shall eventually be adapted on site. Within our navigation system for liver surgery [1], [2], surgeons are provided with the pre-operative 3D images, navigated US imaging and a set of optical trackers for the navigation of standard surgical tools. During the surgical intervention, the accuracy of the pre-operative images is reduced due to motions and deformations of the liver. Thus, updating the pre-operative images with the 3D information obtained from US imaging is an important step towards an increase of the navigation system accuracy.

Registration of CT images with US imaging is usually performed by detecting corresponding features in both data types. A non-rigid transformation can then be computed and applied onto the CT images like in [3]. The most obvious common features between CT- and US- images are liver vessels. They are easily segmented pre-operatively in the CT images, whereas the segmentation of vessels in US images is more challenging as these images have a low signal-noise ratio. Furthermore, it is strongly desirable that the segmentation happens in real-time in order to provide surgeons with direct feedback on the quality of the acquired US information. Several groups have reported on US segmentation algorithms in liver surgery [4] but most of them focused on tumor detection. Recently, [5] showed an algorithm for vessel segmentation and tracking, which requires an initial manual segmentation to start. A dynamic texture approach was presented in [6]. Good segmentation results are reported but again, user intervention is required for tissue classification. In [7] a vessel segmentation algorithm was developed and tested on several porcine livers under isolated perfusion. This segmentation algorithm gave promising results both in terms of efficiency and computational time and does not require user interaction. Within this paper we present the integration of this segmentation algorithm in our navigation system and the initial results of its use in real conditions.

2 Methods

A. Navigation System and Ultrasound Device

The surgical navigation system is built as a transportable setup containing an NDI Vicra Camera (Northern Digital Inc, Canada), an integrated Terason T3000 ultrasound system with an 8IOA intra-operative probe (Teratech Corporation, USA) and a Shuttle barebone PC (Shuttle Inc, Taiwan) with a touch-screen monitor (ELO Touchsystems, USA). Instrument tracking is enabled by a navigation toolset composed of adapters to the existing surgical tools (CUSA, ablation devices, US probe) and a pointer calibration unit.

B. Workflow

Before each navigated liver surgery, pre-operative tri-phase CT data was processed by MeVis Distant Services. The MeVis analysis provides segmentation of all the important structures (vessels, tumors, surface) as well as several resection proposals. The resulting 3D models are evaluated by the surgeons and appropriate visualization models are selected and loaded into the navigation system.

The navigated surgery starts by an initial rigid registration of the liver. Four landmarks are manually defined on the virtual liver model. Then, the tip of the CUSA is calibrated with the pointer calibration unit. Using the CUSA tip, the surgeon points the four manually defined landmarks on the real liver, which are automatically recorded by the navigation system. Through the alignment of these two point sets, initial rigid registration is obtained.

In a second stage, US images are acquired and segmented in real-time. The US probe is pre-calibrated using an US calibration unit pre-operatively [8]. Using the probe, vessels are traced by the surgeon. The obtained segmentation and images are recorded with the corresponding position tracking information for further data analysis.

C. Vessel Segmentation

The vessel segmentation algorithm is based on the approach proposed by Dagon in [7] may be shortly described as:

1. Vessel image mask generation
2. Vessel seed point detection
3. Vessel approximation using an elliptical model
4. Outliers removal

The vessel mask generation starts with a scale-space blob detection [9], which is performed by generating scale-space images I_l with eight different scale levels S_l using a Gaussian Kernel of:

$$\sigma = 3 \cdot S_l \tag{1}$$

The pixel intensities of the scale-space images are then summed in a scale-space map I_{Map} with the following equation:

$$I_{Map}(x, y) = \sum_{l=1}^{n} \left[I_n(x, y) - I_l(x, y) \right] \tag{2}$$

Thus, dark features in the US image that present a large scale-space lifetime are enhanced. A binary threshold t_{sc} is then applied on the scale-space map to obtain the features binary mask I_{Mask}.

The features mask is then cross-correlated with a binary circular mask of radius r_c and normalized. A threshold t_{corr} is applied on the obtained image and a connected component labeling algorithm is run in order to identify the highest intensity pixel in each region, which is then labeled as seed point.

To approximate the blood vessel, an elliptical model is applied. To detect the vessel border, rays are regularly casted around the seed point on the initial scale-space mask I_{Mask}. The edge points are detected at the first value change in the ray intensity profile. The edge points are then used to initialize a direct least square ellipse fitting algorithm [10], [11].

Finally, outliers are filtered by defining minimal and maximal ellipse axes ratio and axes average length.

The C++ implementation of the segmentation algorithm was based on the code provided by Dagon [7] which was improved by adding outlier removal in the vessel seed point detection step and by integrating a region of interest (ROI) provided by the direct interface to an US imaging device (described in Section 2.D)

D. Software integration

The segmentation algorithm was integrated into our navigation software [1],[2]. In this way, the segmentation is applied in real-time onto the images generated by the US probe. The obtained segmentation is visualized in both the 2D US image and in the 3D world viewer. A touch-screen user interface was developed for easy use in the operation room environment. The user can switch the segmentation algorithm on and off, change segmentation parameters and record both

US images and the obtained segmentations. The segmentation steps can be visualized to better understand the parameters respective influences (Fig. 1). The whole sequence can be loaded and segmented again later with different parameters.

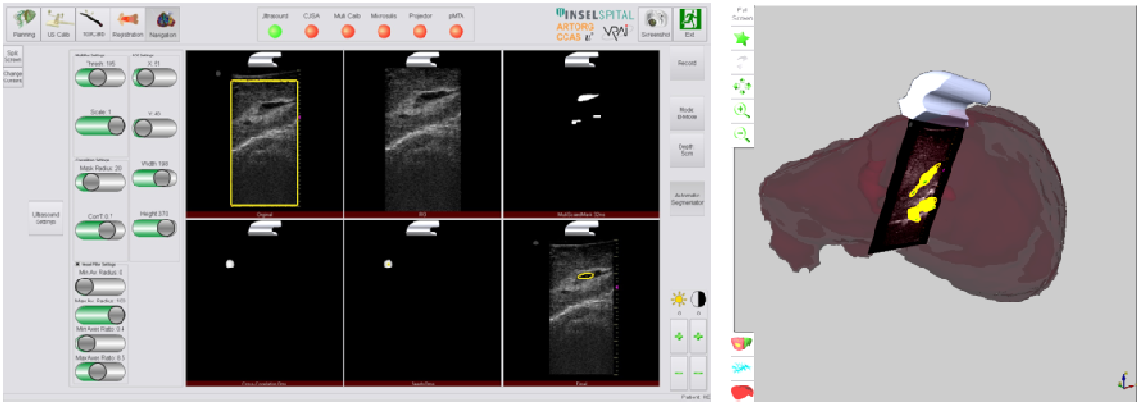

Fig. 1: Navigation software: On the left side, the user interface in detailed mode displays each step of the segmentation algorithm (original image, ROI, scale-space, correlation, seed points, ellipse fitting). On the right side, the 3D view shows the pre-operative image, tracked US probe and the segmentation (yellow).

E. Validation

A validation application was developed for the result analysis. The recorded US images are loaded again with the obtained automatic vessel segmentation centers. The user then manually defines whether the detected vessel centers are correct, wrong (false positive) or missing (Fig. 2, right). The application then outputs the total number of each vessel center classification.

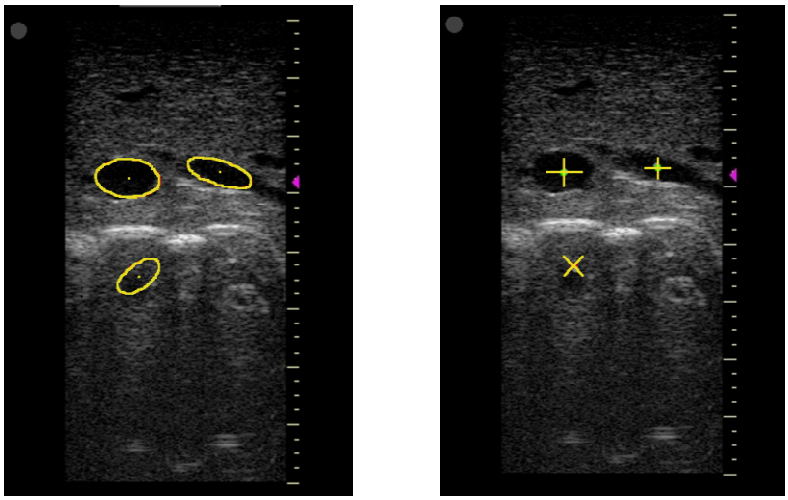

Fig. 2: Typical vessel detection produced by the vessel segmentation algorithm (left). Two segmented vessels are correct (+) and one is wrong (x) (right).

3 Results

About 2’200 images (300x430 pixels) were recorded and segmented during one surgical intervention at the Inselspital in Bern, Switzerland. The US probe parameters for brightness, contrast and time gain control were set to the default values. The average time to process one image was 70ms, which resulted in a frame rate of 7 frames per second. Six subsets including a total of 538 images were selected for post-operative analysis with optimized segmentation parameters. Table 1 and 2 present the results obtained with the parameters: t_{sc} = 65, r_c = 10 pixels, t_{corr} = 0.01, Region of Interest: 193x371 pixels.

	Processed images	Expected vessel centers	Correct centers	Missing centers
Set 0	109	551	250	301
Set 1	42	107	55	52
Set 3	147	463	223	240
Set 6	73	265	73	192
Set 10	13	26	22	4
Set 12	154	408	278	130

Table 1: Amount of correct- and missing- centers compared to the number of expected vessels.

	Processed images	Vessels detected	Correct classification	Wrong classification
Set 0	109	374	250	124
Set 1	42	158	55	103
Set 3	147	421	223	198
Set 6	73	228	73	155
Set 10	13	25	22	3
Set 12	154	295	278	17

Table 2: Amount of correct- and wrong- centers compared to the number of detected vessels.

The average value of correctly classified vessels is 60.03%. The average number of missing vessels per frame is 1.7 and the average value of wrongly classified vessels per frame is 1.1.

4 Discussion

The number of missing vessels per frame is relatively high and is mainly caused by small vessels. When the threshold value t_{sc} is set to a low value, small vessels are better detected but the amount of wrongly classified vessels from image noise increases as well. Wrongly classified vessels come from homogeneous noise regions in the images and from artefacts lying under the liver borders as illustrated in Fig. 2. When comparing our results with the ones presented by Dagon [7], we see improved outcomes in the amount of correctly segmented vessels (40% by Dagon, 60% in this work). However, the results are not directly comparable as different image data and slightly different validation methodologies were used. The images used herein were acquired in real surgery on human patients where Dagon used an ex-vivo porcine liver specimen under isolated perfusion. The validation approaches differ in that the distance between the manual and automatic segmented vessel centers was not considered for the vessel classification within this work. The higher computation time of 70ms vs 25ms in this work can be explained by the larger size of the US images used with the Terason imaging device and the added load due to the visualization of the segmentation steps as shown in Fig. 1.

As we aim to use the segmentation results for intra-operative registration, a further reduction of wrongly classified vessels is desirable. This should be partly solved by detecting the lower organ borders. Another way for reducing wrongly classified vessels is to use the 3D position information of the segmented vessels in the prior images to predict their positions in the next frame. In general, the large number of segmentation parameters made it difficult to obtain a good segmentation while in the operating room. Reducing their number or an automatic adjustment of some parameters might solve this issue.

Another effect observed when comparing the segmentation results from different acquisitions is the high sensitivity to the US image quality. We believe that by adjusting the US imaging parameters, in particular brightness, contrast and time gain control, the number of missing vessels per frame should decrease. The development of the vessel-based registration methods will show whether a reliable detection of large vessels or detection of smaller vessels with higher error rate are preferable.

Finally, the computation time of 70ms per frame is not yet acceptable for a real-time application. Considering that there should be more processing for the registration afterwards. This should be improved by code optimization and/or using GPU computing or multi-threading.

5 References

[1] M. Peterhans, B. Dagon, L. Nolte, C. Baur, A. Vom Berg, D. Inderbitzin, and S. Weber, “Soft tissue navigation: Transfering operative planning data into the operation room”, ECR 2009 Book of Abstracts, 2009.

[2] A. Vom Berg, D. Candinas, D. Inderbitzin, M. Peterhans, S. Weber, and L. Nolte, “Computer assisted surgery and navigation in complex hepatic surgery and tumorablation: first clinical results of 10 patients”, Proceedings of CARS 2010, 2010.

[3] T. Lange, N. Papenberg, S. Heldmann, J. Modersitzki, B. Fischer, H. Lamecker, and P.M. Schlag, “3D ultrasound-CT registration of the liver using combined landmark-intensity information,” IJMRCAS, 2009.

[4] J. A. Noble, and D. Boukerroui, “Ultrasound Image Segmentation: a Survey”, TMI, 2006.

[5] J. Guerrero, S. E. Salcudean, J. A. McEwen, B. A. Masri, and S. Nicolaou, “Real-Time Vessel Segmentation and Tracking for Ultrasound Imaging Applications”, TMI, 2007.

[6] S. Milko, E. Samset, and T. Kadir, “Segmentation of the liver in ultrasound: a dynamic texture approach”, IJMRCAS, 2008.

[7] B. Dagon, C. Baur, and V. Bettschart, “Real-Time Update of 3D Deformable Models for Computed Aided Liver Surgery”, Proceedings of IAPR, 2008.

[8] M. Peterhans, S. Anderegg, P. Gaillard, T. Oliveira-Santos, and S. Weber, “A Fully Automatic Calibration Framework for Navigated Ultrasound Imaging”, Accepted for Proceedings of EMBC 2010, 2010.

[9] T. Lindeberg, “Detecting Salient Blob-Like Image Structures and Their Scales with a Scale-Space Primal Sketch: A Method for Focus-of-Attention”, International Journal of Computer Vision, 1993.

[10] A. Fitzgibbon, M. Pilu, and R. B. Fisher, “Direct Least Square Fitting of Ellipses”, 13th International Conference on Pattern Recognition, 1996.

[11] R. Halir and J. Flusser, “Numerically Stable Direct Least Squares Fitting of Ellipses”, 1998.